Aust. Met. Mag. 47 (1998) 135-144

A monsoon depression over northwestern Australia part II: a numerical model study

Klaus Dengler and Roger K. Smith
Meteorological Institute, University of Munich, Munich, Germany

(Manuscript received February 1997; revised November 1997)

A numerical shallow-water model is used to investigate dynamical aspects of the evolution of an initial weak and broad vortex circulation in the absence of a basic flow. The initial vortex lies partly over land and is centred over the coast which is straight and runs from southwest to northeast. The situation is relevant to the case study of the development of a monsoon depression near the northwestern coast of Australia presented in Part I. The model incorporates a modified form of the convective parametrisation scheme developed by Ooyama. The modifications were found to be necessary when the cyclonic circulation has its centre in the proximity of land.

On an f-plane the initial vortex intensifies to a strength comparable to that of the observed monsoon depression and moves eastwards over the land. The eastward drift is caused by asymmetries in the convection which are a result of the land-sea distribution. On a beta-plane the motion is dominated by the flow associated with the beta-induced vorticity asymmetries and the vortex moves southwestwards and further inland. Accordingly, its maximum intensity is less than that on the f-plane. On a beta-plane in the absence of land, the vortex attains the strength of an intense tropical cyclone with maximum winds of 48 m s^{-1} and drifts towards the southwest.

Introduction

An appreciable amount of rainfall in the Australian tropics is associated with monsoon depressions and these systems pose a significant forecasting problem in the region, especially since they may evolve into tropical cyclones when they move out over the ocean (McBride and Keenan 1982). In Part I of this study, Hell and Smith (1998) analyse a case of a monsoon depression which formed in the monsoon trough near the northwest coast of Australia and whose development was not anticipated by forecasters. The event is of particular dynamical interest because, during the period of rapid development, the depression remained quasi-stationary and its centre lay close to the coast. Moreover, there appeared to be little obvious influence on its development from neighbouring disturbances as in other reported case studies in the region. After a few days the depression drifted slowly towards the southwest. The drift direction was similar to that of an isolated barotropic vortex, and aspects of the motion will be analysed in detail by Weber and Smith in a forthcoming paper (Part III). In this paper we describe some simple numerical model experiments relevant to the case study in Part I.

There have been relatively few theoretical investigations of monsoon depressions, although a copious literature exists on the dynamics of middle-latitude depressions. Nevertheless, there have been a few numerical studies of monsoon depressions focusing on the Indian region (e.g. Shukla 1978; Mishra and Salvekar 1980; Aravequia et al. 1995) and we review briefly these and other related studies below.

Shukla (1978) used a CISK*-barotropic-baroclinic instability analysis of the monsoon flow using a numerical three-layer quasi-geostrophic model. The model employed the quasi-equilibrium assumption introduced by Arakawa and Schubert (1974) to parametrise cumulus convection. Shukla found that the maximum growth rate occurs for the smallest scales and attributed this to either the inadequate formulation of the subcloud layer or to the parametrisation of convection in the model. He found also that latent heating by cumulus convection is

Corresponding author address: Prof. Roger K. Smith, Meteorological Institute, University of Munich, Theresienstr. 37, 80333 Munich, Germany.

* Conditional Instability of the Second Kind (see e.g. Smith 1997).

the primary energy source of the monsoon depression while baroclinic instability plays only a secondary role. In his calculations, the CISK process seems to determine the magnitudes of the growth rate and the dominant energy transformations.

Aravequia et al. (1995) investigated the effect of the vertical heating structure on baroclinic instability in the presence of different zonal wind shears. Using a double maximum in the vertical heating profile, which they note is appropriate for the monsoon case, they found that the most unstable wave had a vertical structure similar to that of observed monsoon depressions. Their study is an extension of the work by Moorthi and Arakawa (1985) who investigated the effects of cumulus heating on the baroclinic instability of zonal flows with easterly and westerly shears.

Numerical investigations of the transformation of an easterly wave into a tropical storm and the influence of an environmental flow on tropical storm genesis have been performed by Kurihara and Tuleya (1981), Tuleya and Kurihara (1981) and Kurihara and Kawase (1985). The first two studies used an eleven-level primitive equation (PE) model with a moist convective adjustment scheme developed by Kurihara (1973). Kurihara and Tuleya found that boundary-layer convergence induces upward motion in the wave trough and that the region of ascent extends upward with time. This development is accompanied by a deepening of the convergence layer around the depression centre and the formation of a warm core, as in tropical cyclones. The warming process appears first in the upper troposphere and extends downwards as the development progresses. A heat budget shows that warming by latent heat release in cumulus clouds slightly exceeds the adiabatic cooling of the rising air and is responsible for the development of the warm core. Tuleya and Kurihara showed that when the mean surface flow is easterly, easterly vertical shear (i.e. easterlies increasing with height) of moderate magnitude (e.g. 15 m s^{-1} between 850 and 150 hPa) is conducive to storm genesis, whereas westerly shear of comparable magnitude is detrimental to genesis.

In an attempt to isolate some of the basic processes involved in tropical cyclogenesis Kurihara and Kawase used a simpler two-dimensional PE-model on a beta-plane. In this model an easterly wave was represented by an adiabatic normal mode of the linearised equations for a basic easterly zonal flow. The wave is essentially a Rossby-wave mode and was chosen to have its maximum amplitude at low levels. Cumulus heating was assumed to be proportional to the mean divergence in the lowest two model levels (1000 hPa and 900 hPa). Calculations showed that development did not occur if the cumulus scheme was switched off, irrespective of the presence or absence of the nonlinear terms in the equations, but the inclusion of the nonlinear terms accelerated the wave growth in the presence of diabatic forcing. The inference is that latent heat release is the primary process for the development of the tropical depression as was suggested by Shukla (1978). A critique of Kurihara and Kawase's paper was given by McBride and Willoughby (1986).

All of the foregoing studies consider cyclone development over the ocean in a zonal basic flow. In the present paper we investigate dynamical aspects of the evolution of an initially weak and broad vortex circulation in the absence of a basic flow. In the two main calculations, the vortex centre is located initially over the coast so that the circulation lies partly over land. This situation is relevant to the monsoon depression investigated in Part I and the choice of vortex size, scale and location is guided by the observations of this disturbance in its early stage of development. The study uses a three-layer numerical, shallow-water model with parametrisations of friction, convection and sea-surface energy exchange. The model is described in Dengler and Reeder (1997; hereafter DR97) who used it to investigate the motion of tropical cyclones. The cumulus parametrisation scheme is a modified version of that proposed by Ooyama (1969), the modifications being required when the scheme is applied over land where the latent heat energy supply from the surface is effectively cut off (or at least significantly reduced).

The model is described briefly in the next section along with the cumulus parametrisation scheme. Subsequent sections describe the experiments that are carried out and the results of these calculations. The final section presents a summary and conclusions.

The numerical model

We use a three-layer shallow-water model for the calculations. The model is an extended version of that developed by Ooyama (1969) and is described in detail in DR97. The model layers are homogeneous and their undisturbed depths and densities are: 870 m and 1.17 kg m^{-3} for the boundary layer (layer 3), 3800 m and 1.11 kg m^{-3} for the middle layer (layer 2) and 3700 m and 0.96 kg m^{-3} for the upper layer (layer 1)* . The depths are chosen to give the same vertical stratification as used by DR97. The prognostic equation for the layer depths including that of the boundary layer is given by

$$\frac{\partial h_i}{\partial t} + \nabla_h \cdot (h_i \boldsymbol{u}_i) = Q_i \qquad \ldots 1$$

where h_i is the depth of layer i (i = 1,2,3), $\boldsymbol{u}_i$ is the horizontal wind vector, and Q_i is a mass source/sink term in this layer.

* The numbering of the layers follows Ooyama (1969).

The heating effects of deep cumulus convection are represented by a transport of mass from the boundary layer into the upper layer in regions of boundary-layer convergence as indicated schematically in Fig. 1. Moreover, they enter the formulation entirely through the specification of Q_i in Eqn 1. The mass transfer is accompanied by entrainment from the middle layer so that for each unit of mass that leaves the boundary-layer, (η - 1) units are entrained and η units are deposited in the upper layer (η is the non-dimensional vertical stability parameter defined below). The mass transferred carries with it the momentum characteristic of its source level. In regions of boundary-layer divergence, mass and momentum are transported from the middle layer into the boundary layer. The momentum equations are given in DR97.

In the region of boundary-layer convergence, the expression for Q_i is:

$$Q_i = \begin{cases} \frac{\rho_3}{\rho_1}\,\eta w^+_{*5/2} & \text{if } i = 1 \\ (1-\eta)\,\frac{\rho_3}{\rho_2}\,w^+_{*5/2} & \text{if } i = 2 \\ -w^+_{*5/2} & \text{if } i = 3 \end{cases} \qquad ...2$$

where ρ_i is the density of layer i, and $w^+_{*5/2}$ is the vertical motion at the top of the boundary layer. The coefficient 1 - η in Q_2 represents the rate of entrainment of middle-layer air*.

The simplicity of the model is such that the flow evolution is determined once a suitable expression for η is obtained. The following equivalent expressions for η are determined by a simple energy budget for the convective updraught:

$$\eta = 1 + \frac{\Lambda_3 - \Lambda_1^*}{\Lambda_1^* - \Lambda_2} = \frac{\Lambda_3 - \Lambda_2}{\Lambda_1^* - \Lambda_2} \qquad ...3$$

where Λ_i is the moist static energy of layer i and Λ_1^* is the saturated moist static energy of the air in the detrainment layer, layer 1. The difference $\Lambda_3 - \Lambda_1^*$ in Eqn 3 can be regarded as a local measure of the degree of convective instability in the model, the condition $\Lambda_3 \geq \Lambda_2^* \geq \Lambda_2$ being required for convection to occur between levels 3 and 2 and $\Lambda_2 \geq \Lambda_1^*$ being required for convection to occur between levels 2 and 1 (see e.g. Haltiner (1971) section 10.4). In a neutral atmosphere, $\Lambda_3 = \Lambda_2^* = \Lambda_1^*$ and $\eta = 1$.

The quantity Λ_3 depends on the boundary-layer moisture content, represented by the mixing ratio r_3. Thus, in addition to the shallow-water equations, the model incorporates a prognostic equation for r_3 (see DR97), although this quantity is used only to determine η: it enters the dynamical problem only in as much as it determines the degree of conditional instability through the vertical distribution of Λ. The energy transfer from the ocean into the boundary layer is given by

$$Q_{Sc} = \frac{c_E\,|\boldsymbol{u}_3|}{h_3}\,(r_s - r_3) \qquad ...4$$

where c_E is a non-dimensional energy exchange coefficient, h_3 is the depth of the boundary layer, $\boldsymbol{u}_3$ is the horizontal wind and r_s is the saturation mixing ratio in the boundary layer.

The convective scheme is intended to represent deep convection only and relates to the situation where $\eta \geq 1$ shown in Fig. 1(a). In simulations of tropical cyclones, this condition is always satisfied as long as the vortex remains over the ocean and is deepening. When $\eta = 1$, the air rising out of the boundary layer is transported into the upper layer without entraining middle-layer air (Fig. 1(b)). Values of η close to unity reflect conditions in the mature stage of a tropical cyclone when the convection is close to conditionally neutral.

In situations where there is land present in the vicinity of the vortex, there exist regions of boundary-layer convergence where $0 \leq \eta < 1$. If the original Ooyama scheme is used in such regions, a fraction of the boundary-layer air would be transported into the upper layer, and a fraction would be detrained into the middle layer. In extreme cases, when the air has a long trajectory over land, it is possible that $\eta < 0$, implying that air descends from the upper layer into the middle layer. Although mass conservation still holds in these situations, the parametrisation scheme is clearly unrealistic. Indeed, if $\eta < 1$, the atmosphere is stable to deep convection since $\Lambda_1^* > \Lambda_3$ (see Appendix A in DR97). To avoid these unrealistic situations, the convection scheme is switched off if $\eta < 1$. Therefore, if $\eta < 1$ in regions of boundary-

Fig. 1 **Vertical motion in regions of boundary-layer convergence for different values of η: (a) $\eta > 1$ (deep convection and deepening stage of tropical cyclone); (b) $\eta = 1$ (deep convection and mature stage).**

* For details the reader is referred to Dengler and Reeder (1997).

layer convergence, mass and momentum are transported from the boundary layer into the middle layer only. An alternative would be to suppress any mass transfer from the boundary layer if $\eta < 1$ so that air accumulates in the boundary layer, which locally thickens. However, tests showed that this leads to the development of large and unrealistic boundary-layer thicknesses with vertical displacements which would lead to convection in reality.

The model is energetically consistent in that the mass transfer between layers generates available potential energy which is converted to kinetic energy, and, in turn, this suffers dissipation on account of surface frictional stresses. However, because it consists of homogeneous layers, the model contains no explicit representation of internal energy; i.e. all thermodynamic processes are implicit in the model and enter the formulation entirely through the specification of η as explained above. It turns out that this leads to rainfall estimates which are lower than those that are typically observed in hurricanes. A careful discussion of the energetics is provided by Ooyama (1969).

Initial conditions and experimental design

The initial vortex is cyclonic and has maximum tangential winds of 10 m s^{-1} at a radius of 400 km in the lower two layers while the upper layer is initially at rest. The tangential wind profile is that used by Smith et al. (1990). Its strength and size are comparable to those of a weak southern hemisphere monsoon depression. The initial environment is the same as in Section 4a of DR97, except that the upper-layer potential temperature is increased to 345K to reduce the amount of environmental CAPE and to emphasise the importance of surface fluxes. Furthermore the sea-surface temperature has been increased from 28°C to 30°C, reflecting the temperature observed off the northwest coast of Australia. The initial value of η is 1.4.

The land-ocean distribution is shown in Fig. 2. Land conditions are assumed on the poleward side of a southwest to northeast oriented line passing through the centre of the initial vortex while the ocean is located equatorward of this line. This configuration is an approximation to the early stages of the monsoon depression studied in Part I which developed near the northwest coast of the Australian continent. Over the ocean the drag coefficient c_D, and energy exchange coefficient c_E, both equal 0.0015, while over land c_D is increased to 0.005 and c_E is set to zero. In the absence of previous recent heavy rainfall, the assumption that $c_E = 0$ seems a reasonable first approximation for the arid region of the northwestern part of Australia, but it clearly represents one extreme of a range of possible

Fig. 2 Ocean-land distribution used in the numerical calculations. The hurricane symbol denotes the centre of the initial vortex.

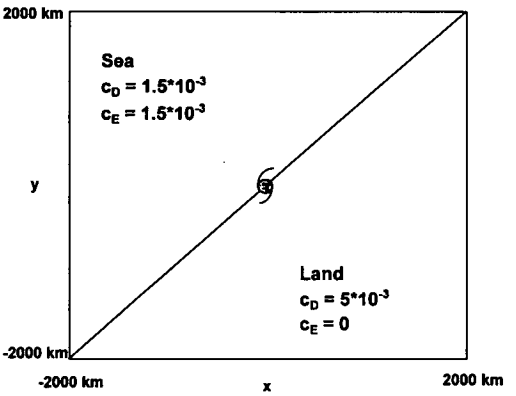

intermediate values less than that over the sea. A domain size of 4000 x 4000 km^2 with a horizontal resolution of 20 km is used for the calculations. In all experiments the initial vortex is centred in the middle of the domain over the coastline at 15°S.

Three numerical experiments are discussed in detail; these are summarised in Table 1. The first one examines the spin-up of the weak initial vortex on a southern hemisphere f-plane centred at 15 °S and is referred to as M1. The second experiment, M2, examines the spin up of the same initial vortex, but on a southern hemisphere ß-plane centred at 15 °S. Finally, the third experiment, M3, is a repeat of experiment M2 with only an ocean surface.

Throughout this work, the location of the minimum surface pressure is used to characterise the vortex centre. This is because the land-sea distribution leads to a highly asymmetric distribution of convective heating, which, in turn, produces a highly asymmetric vorticity distribution, in some cases with more than one local minimum.

Table 1. The numerical experiments.

	M1	*M2*	*M3*
Land	yes	yes	no
Plane	f-plane	ß-plane	ß-plane

Results

Evolution and motion on an f-plane

We consider first the intensification of the initial vortex detailed in the previous section on an f-plane in the presence of land (M1). The evolution of maximum middle-

layer winds and minimum sea-surface pressure in this experiment are shown by the solid lines in Figs 3(a) and (b) respectively. After 60 h, maximum winds of 17 m s^{-1} and 21 m s^{-1} are attained in the boundary layer and middle layer, respectively, and the minimum sea-surface pressure has decreased by about 10 hPa to a value of 996 hPa. The circulation is widespread with gale-force winds extending about 300 km from the vortex centre and maximum wind about 180 km from the centre.

Panels (c) and (d) in Fig. 3 show the dependence of the evolution on the strength of the initial vortex. In addition to M1 (solid line), calculations for initial wind speeds of 7 m s^{-1} and 15 m s^{-1} were carried out. The major differences between the calculations are in the rate of development and the maximum intensity attained: the weaker the initial vortex, the later the mature stage is reached and the weaker is the maximum intensity.

Fig. 3 **Time evolution of (a) maximum middle-layer wind speed and (b) minimum sea-surface pressure for experiments M1 (solid line), M2 (marked 'La') and M3 (marked 'Oc'). The time evolution is shown in (c) and (d) as a function of the strength of the initial vortex. The solid line is for the case M1.**

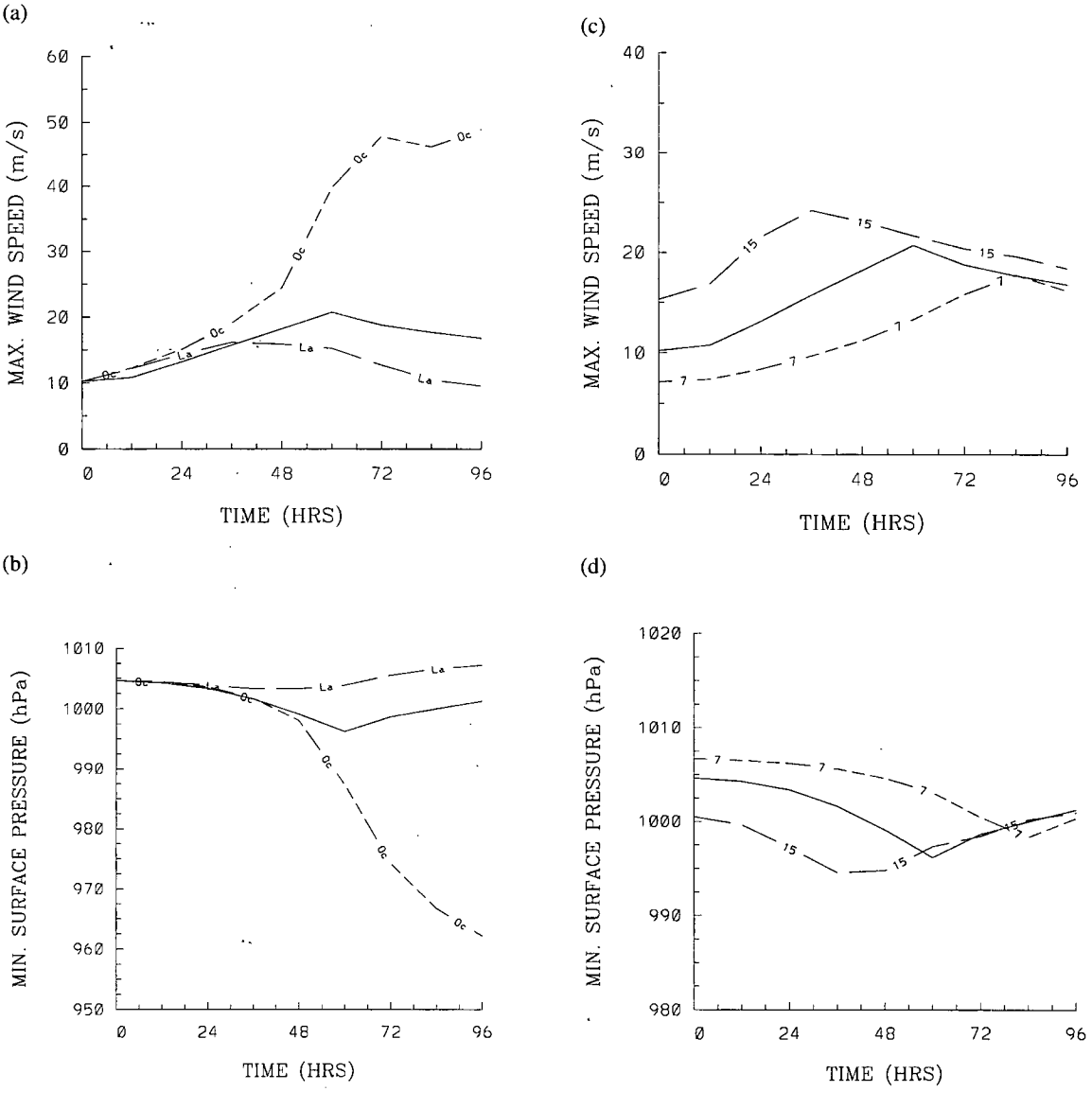

Figure 4(a) shows the surface fluxes (Q_{Sc}) from the ocean into the lower troposphere at 36 h for the case M1, calculated using Eqn 4. Recall that a constant c_E is assumed. The maximum value occurs close to the coastline southwest of the vortex centre (hurricane symbol). The sharp cut-off along the coast is a result of the assumption that surface fluxes are zero over land. The maximum surface fluxes of 14 g kg^{-1}d^{-1} occur in the region of offshore winds southwest of the vortex centre where dry air is advected over the ocean. It is the thermodynamic disequilibrium of the boundary-layer air that is largely responsible for the high values of surface fluxes, not the boundary-layer wind speed. The maximum boundary-layer wind speed is observed to the north of the vortex centre (see wind vectors in Fig. 4(a)). If c_E is assumed to be a function of wind speed, the maximum values of Q_{Sc} increase by about 20 per cent and the intensification rate of the vortex increases, but the horizontal pattern of Q_{Sc} is unchanged. The vertical stability parameter η at 36 h is shown in Fig. 4(b). The thick contour line is where $\eta = 1$ and therefore deep convection is in an exactly neutral state with zero CAPE (see also Fig. 1(b)). Deep convection takes place in regions of boundary-layer convergence to the left of this line where $\eta \geq 1$. Although surface fluxes are high in the region of offshore winds (Fig. 4(a)), the very dry boundary-layer air originating over the continent requires about 350 km fetch over the sea before it is moistened sufficiently for the sounding to become locally convectively unstable ($\eta > 1$): see Fig. 4(a).

Fig. 4 **(a) Sea-surface energy fluxes calculated from Eqn 3 using a constant energy exchange coefficient c_E for case M1 including boundary-layer wind vectors. Contour interval is 1 g kg^{-1} d^{-1}. The hurricane symbol marks the vortex centre which is defined as the location of the minimum geopotential in the middle layer. (b) Non-dimensional vertical stability parameter η for case M1. The thick line shows where $\eta = 1$. Contour interval is 0.2.**

(a)

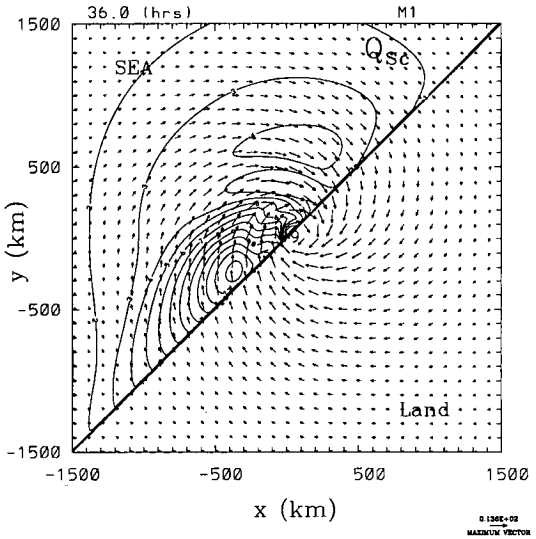

(b)

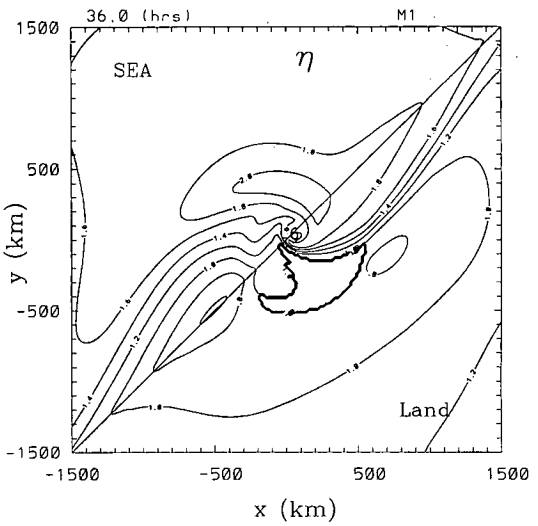

Over land, the minimum relative humidity in the boundary layer is about 45 per cent. For this reason, over land as well as in the region of offshore winds, η has values close to zero. In regions where there is boundary-layer convergence and where $\eta < 1$, the original parametrisation scheme of Ooyama would be unrealistic. To show where this would occur, the mass source/sink term Q_i in regions of boundary-layer convergence (Eqn 2) at 36 h is plotted in Fig. 5.

Figure 5(b) shows that south of the vortex centre, air is detrained into the middle layer ($Q_2 > 0$). Since no air can move from the upper layer into the middle layer ($Q_1 > 0$, see Fig. 5(c)), the mass detrained in the middle layer originates from the low layer ($Q_3 < 0$, see Fig. 5(a)). This is the region where values of $\eta < 1$ coexist with boundary-layer convergence. In this region it is assumed that all air leaving the boundary layer is detrained into the middle layer. In the remaining region, where $Q_3 < 0$, only deep convection with entrainment of middle-layer air occurs.

The vortex track is shown in Fig. 6(a) where it is labelled with a hurricane symbol. During the 96 h integration, the middle-layer vortex moves about 270 km towards the east at an average drift speed of about 0.8 m s^{-1}. The vortex in the boundary layer moves broadly in the same way. This movement over the land reduces the supply of moisture from the sea surface to the vortex core, thereby inhibiting further development. Since in an environment at rest on an f-plane

Fig. 5 **Mass source and sink term Q_i using Eqn 2 for (a) boundary layer, (b) entrainment layer and (c) detrainment layer. Contour intervals are 0.01 m s^{-1} in (a) and (b) while 0.02 m s^{-1} is used in (c). Broken lines denote negative values.**

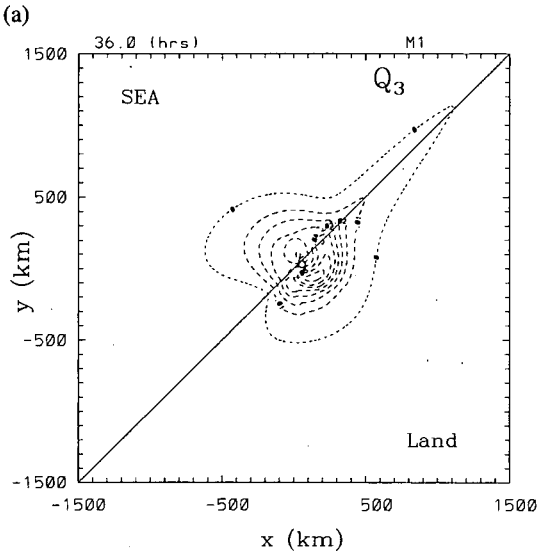

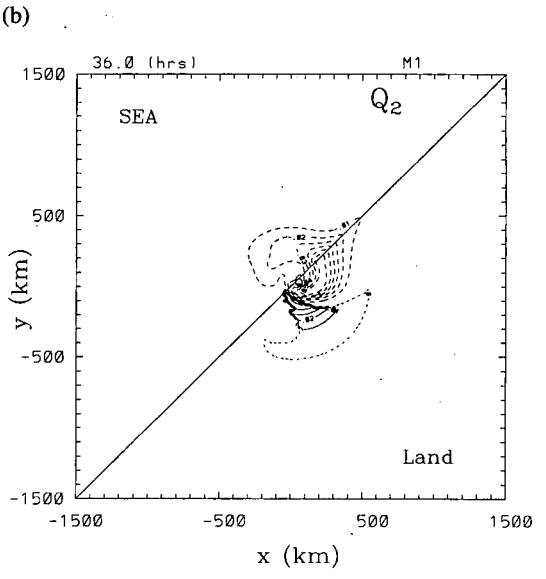

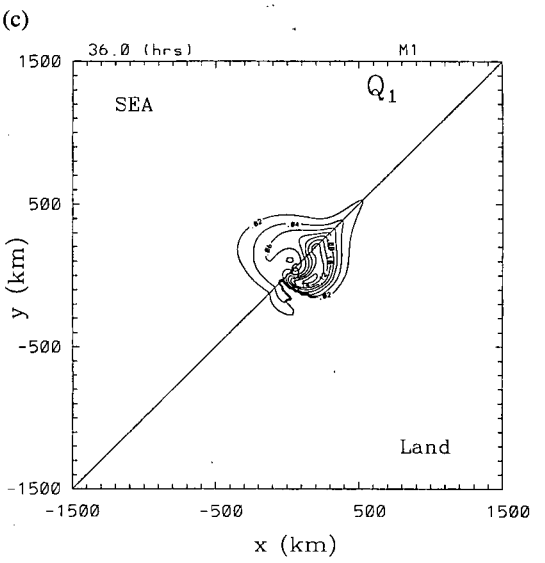

there is no background PV-gradient, the vortex motion must be wholly a result of the flow asymmetry produced by the asymmetric convection arising from the land-ocean distribution.

The strongest boundary-layer convergence is always found to be to the southeast of the vortex centre (not shown). This is the region where the onshore surface winds transport moist air from the ocean over the land where it penetrates close to the cyclone centre (see Fig. 4(b)). The strongest convective activity is found there, leading to a second minimum of relative vorticity in the middle layer located about 250 km to the southeast of the vortex centre. This is best illustrated in the middle-layer vorticity field after 96 h (see Fig. 6(b)). The flow associated with this asymmetry across the vortex centre is responsible for the eastward motion of the cyclone.

Evolution and motion on a ß-plane

Experiment M2 is a repeat of experiment M1 on a southern hemisphere ß-plane centred at 15°S. The development of the vortex in this experiment is indicated by the broken line marked 'La' in Fig. 3. Maximum middle-layer winds of 16 m s^{-1} and a minimum surface pressure of 1000 hPa occur after 36 h. Thereafter the vortex intensity decreases to about 10 m s^{-1} and 1005 hPa after 96 h.

The vortex track, labelled with a star symbol, is shown in Fig. 6(a). During the 96 h integration, the middle-layer vortex moves about 860 km to the south-southwest at an average drift of 2.5 m s^{-1}. The drift is comparable to that of the monsoon depression studied in Part I. Again, the movement over land is responsible for the subsequent decrease in intensity.

As a result of the meridional PV-gradient associated with ß, the poleward advection of high PV-air east of the vortex centre and the equatorward advection of low PV air west of the centre create asymmetries in the vorticity field additional to those produced by asymmetric convection. The total asymmetry in the relative vorticity field in the middle layer after 36 h of integration is shown in Fig. 7. It turns out that the beta-induced asym-

Fig. 6 **(a) Tracks of the middle-layer vortices for experiments M1 (hurricane symbol), M2 ('☆' symbol) and M3 ('*' symbol). Symbols are plotted every 24 h. The vortex centre is defined as the location of the minimum geopotential. (b) Relative vorticity in the middle layer after 96 h for the case M1. Contour interval is 1.0 x 10^{-5} s^{-1}. The maximum and minimum values are 4.3 x 10^{-6} s^{-1} and -2.5 x 10^{-4} s^{-1} , respectively. Dashed (solid) contours show negative (positive) values. The vorticity decreases towards the centre, which is marked by the hurricane symbol. Note the second minimum 250 km southeast of this centre.**

(a)

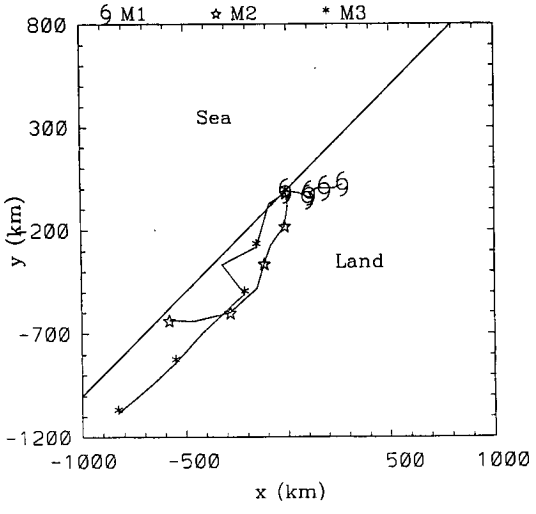

(b)

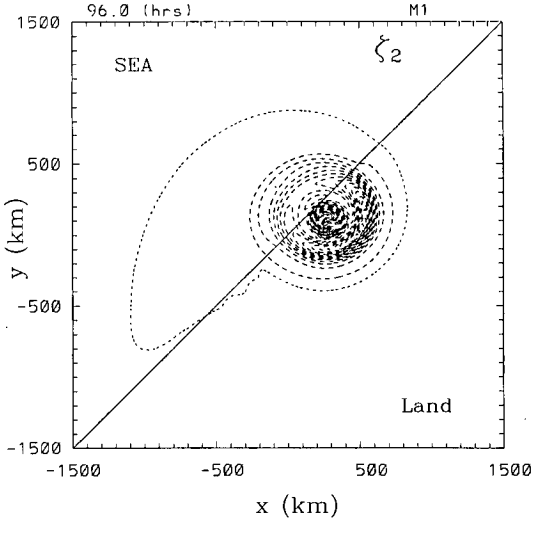

Fig. 7 **Isolines of the relative vorticity asymmetry in the middle layer at 36 h in experiment M2. Contour interval is 5 x 10^{-6} s^{-1}. The maximum and minimum values are 1.6 x 10^{-5} s^{-1} and -1.7 x 10^{-4} s^{-1} , respectively. Dashed (solid) contours show negative (positive) values.**

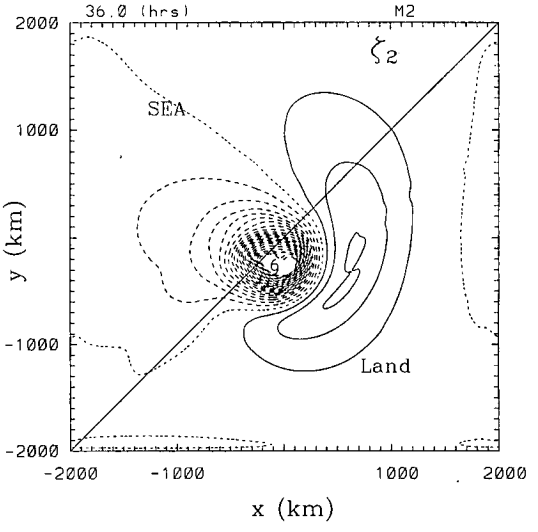

metries make the largest contribution to this flow, in part because they are larger in scale. The structure of these asymmetries is similar to that obtained in the experiments of DR97, taking into account the appropriate sign changes for vorticity in the southern hemisphere. Accordingly, we may surmise that, as in those experiments, the flow associated with the total vorticity asymmetry advects the vortex towards the south-southwest. This flow would be dominated by the large anticyclonic gyre to the southeast of the vortex centre.

Since much of the air circulating around the vortex has a long trajectory over the land, there is a relatively large area where $\eta < 1$ (see Fig. 8) compared with experiment M1. Furthermore, most of the boundary-layer convergence as well as the highest wind speeds occur over land. As a result convective heating is reduced significantly. The mass source/sink fields Q_1 and Q_2 in experiment M2 are similar to those in experiment M1 shown in Fig. 5. In particular, mass is detrained into the middle layer ($Q_2 > 0$) south of the middle-layer vortex centre.

In experiment M3, which is a repeat of experiment M2 over the ocean, the vortex intensifies rapidly into one of tropical cyclone strength with maximum winds around 48 m s^{-1} at the end of the 96 h integration ('Oc' in Fig. 3). This cyclone moves to the southwest at an average speed of 3.7 m s^{-1}. The track is labelled with

Fig. 8 As Fig. 4(b) but for the case M2.

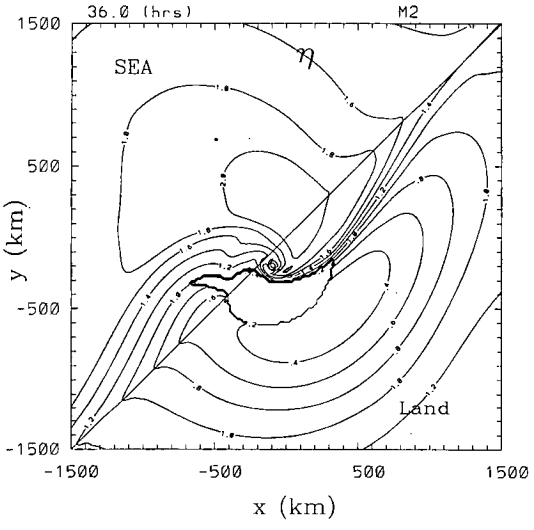

an asterisk in Fig. 6(a). The vortex moves about 450 km further to the southwest than in the case M2 on account of the stronger outer circulation that develops in this case. This, in turn, leads to stronger beta-induced asymmetries.

Summary and conclusion

An incompressible three-layer, numerical shallow-water model with parametrisations of friction, cumulus convection and sea-surface energy exchange has been used to study the dynamics of a monsoon depression. The calculations were motivated by the observational study of a monsoon depression that developed near the coast of northwestern Australia presented in Part I. The aim of this study was to investigate the possible effects of asymmetric convection on the evolution and motion of such a depression using as simple a model as possible.

On an f-plane, in the proximity of land, an initially weak and broad vortex intensifies in the model to one of minimal tropical-cyclone strength with maximum winds of 21 m s^{-1}, comparable to those analysed for the depression in Part I (although the latter was not named a tropical cyclone). As a result of the convectively induced flow asymmetries, the storm moves over land, thereby reducing the surface fluxes and the vortex intensity.

On a beta-plane, the same vortex moves further inland, but in a different direction, intensifying to a maximum of about 17 m s^{-1} before decaying. In this case, the motion is largely a result of flow asymmetries associated with the beta-effect, i.e. with the vorticity anomalies caused by the advection of the background PV-gradient by the cyclonic circulation. On a beta-plane, in the absence of land, the vortex develops into an intense tropical cyclone, with maximum winds of 48 ms^{-1}, and drifts towards the southwest. Thus the presence of land inhibits intensification of the weak initial vortex into a concentrated tropical cyclone strength vortex.

The modelling exercise led us to examine the performance of the Ooyama representation of cumulus heating in the situation when vortex development occurs partly over land. In regions that are unstable to deep convection, the parametrisation scheme transports mass and momentum from the boundary layer into the upper layer (detrainment layer), at the same time entraining mass and momentum from the middle layer (entrainment layer). In the regions of boundary-layer divergence, mass and momentum are transported from the middle layer into the boundary layer. No deep convection is allowed to take place in this region. An analysis of the convective mass fluxes showed that, in its original form, the parametrisation scheme becomes unrealistic over land. This occurs in regions where there is boundary-layer convergence and where $\eta < 1$; then mass and momentum would be transported into the upper layer even though in this case the atmosphere is not convectively unstable. To avoid this difficulty, deep convection is turned off in these regions and boundary-layer air is transported into the middle layer. Future work is continuing to develop a more versatile representation of convection for this situation. The present model with its homogeneous layers would appear unsuitable for this extension and a re-formulation of the model to include an explicit thermodynamic energy cycle is called for.

On account of the simplicity of the model, the results must be regarded as suggestive rather than definitive. However, they highlight some of the key issues in understanding the behaviour of monsoon depressions in the proximity of land and we see them as a useful starting point for a more sophisticated study of these systems using a more complex mesoscale model.

Acknowledgments

This research was supported by the German Research Council (Deutsche Forschungsgemeinschaft), and by the US Office of Naval Research through Grant Nos. N00014-95-I-0394 and N00014-92-J-1532.

References

Aravequia, J.A., Brahmananda Rao, V. and Bonatti, J.P. 1995. The role of moist baroclinic instability in the growth and structure of monsoon depression. *J. Atmos. Sci., 52*, 4393-409.

Arakawa, A. and Schubert, W. H. 1974. Interaction of cumulus cloud ensemble with the large-scale environment. *J. Atmos. Sci., 31*, 673-701.

Dengler, K. and Reeder, M. J. 1997. The effects of convection and baroclinicity on the motion of tropical-cyclone-like vortices. *Q. Jl R. met. Soc., 123*, 699-727.

Haltiner, G.J. 1971. *Numerical Weather Prediction,* Wiley, New York, 317pp.

Hell, R and Smith, R.K. 1998. A monsoon depression over northwestern Australia part I: case study. *Aust. Met. Mag., 47*, 21-40.

Kurihara, Y. 1973. A scheme for moist convective adjustment. *Mon. Weath. Rev., 101*, 547-53.

Kurihara, Y. and Tuleya, R.E. 1981. A numerical simulation study on the genesis of a tropical storm. *Mon. Weath. Rev., 109*, 1629-53.

Kurihara, Y. and Kawase, M. 1985. On the transformation of a tropical easterly wave into a tropical depression: A simple numerical study. *J. Atmos. Sci., 42*, 68-77.

McBride, J.L., and Keenan, T.D. 1982. Climatology of tropical cyclone genesis in the Australian region. *Jnl climate, 2*, 13-33.

McBride, J.L. and Willoughby, H.E. 1986. Comment - An interpretation of Kurihara and Kawase's two-dimensional tropical-cyclone development model. *J. Atmos. Sci., 43*, 3279-83.

Mishra, S.K. and Salvekar, P.S. 1980. Role of baroclinic instability in the development of monsoon disturbances. *J. Atmos. Sci., 37*, 383-94.

Moorthi, S. and Arakawa, A. 1985. Baroclinic instability with cumulus heating. *J. Atmos. Sci., 42*, 2007-31.

Ooyama, K.V. 1969. Numerical simulation of the life cycle of tropical cyclones. *J. Atmos. Sci., 26*, 3-40.

Shukla, J. 1978. CISK-barotropic-baroclinic instability and the growth of monsoon depressions. *J. Atmos. Sci., 35*, 495-508.

Smith, R.K. 1997. On the theory of CISK. *Q. Jl R. met. Soc., 123*, 407-19.

Smith, R.K., Ulrich, W. and Dietachmayer, G. 1990. A numerical study of tropical cyclone motion using a barotropic model. Part I. The role of vortex asymmetries. *Q. Jl R. met. Soc., 116*, 337-62.

Tuleya, R.E and Kurihara, Y. 1981. A numerical study on the effects of environmental flow on tropical storm genesis. *Mon. Weath. Rev. 109*, 2487-506.